RECENT RESULTS FROM THE PEP-4 TPC

LBL--17806

DE84 013241

Ronald J. Madaras

Lawrence Berkeley Laboratory
University of California
Berkeley, CA 94720

Representing the PEP-4 TPC Collaboration*

Presented at the
XIXth Rencontre de Moriond
La Plagne, France, March 4-10, 1984

ABSTRACT

We present here the latest results from the PEP-4 TPC on inclusive charged and neutral particle production, resonance production, heavy quark fragmentation and flavor correlations.

*Members of the PEP-4 TPC Collaboration are:

H. Aihara, R. Avery, M. Alston-Garnjost, D.H. Badtke, J.A. Bakken, H-U.Bengtson, A.Barbaro-Galtieri, A.V.Barnes, B.A.Barnett, B.J.Blumenfeld, A.D.Bross, C.D.Buchanan, O.Chamberlain, C.Chen, J.Chiba, C-Y.Chien, A.R.Clark, A.Cordier, O.I.Dahl, C.T.Day, P.Delpierre, K.A.Derby, P.H.Eberhard, D.L.Fancher, H.Fujii, T.Fujii, B.Gabioud, J.W.Gary, W.Gorn, W.Gu, N.J.Hadley, J.M.Hauptman, H.J.Hilke, W.Hofmann, J.E.Huth, J.Hylen, H.Iwasaki, T.Kamae, H.S.Kaye, R.W.Kenney, L.T.Kerth, R.I.Koda, R.R.Kofler, K.K.Kwong, J.G.Layter, C.S.Lindsey, S.C.Loken, G.W.London, X-Q.Lu, G.R.Lynch, L.Madansky, R.J.Madaras, R.Majka, J.Mallet, P.S.Martin, K.Maruyama, J.N.Marx, J.A.Matthews, S.O.Melnikoff, W.Moses, P.Nemethy, D.R.Nygren, P.J.Oddone, D.A.Park, A.Pevsner, M.Pripstein, P.R.Robrish, M.T.Ronan, R.R.Ross, F.R.Rouse, R.R.Sauerwein, G.Shapiro, M.D.Shapiro, B.C.Shen, W.E.Slater, M.L.Stevenson, D.H.Stork, H.K.Ticho, N.Toge, M.Urban, R.F.van Daalen Wetters, G.J.VanDalen, R.vanTyen, H.Videau, E.Wang, M.R.Wayne, W.A.Wenzel, Z.Wolf, H.A,Yamamoto, M.Yamauchi, M.E.Zeller, W-M.Zhang

Lawrence Berkeley Laboratory, University of California, Berkeley, CA
University of California, Los Angeles, CA
University of California, Riverside, CA
Johns Hopkins University, Baltimore, MD
University of Massachusetts, Amherst, MA
University of Tokyo, Tokyo, JAPAN
Yale University, New Haven, CT

1. INTRODUCTION

The PEP-4 Facility is a large detector complex based on the Time Projection Chamber (TPC), which was developed at the Lawrence Berkeley Laboratory. The TPC is a large-solid-angle compact drift chamber that provides in one detector pattern recognition with three dimensional nonprojective tracking information, and identification of particles by measurement of dE/dx ionization energy loss.

The PEP-4 TPC detector began data taking at the PEP electron-positron colliding beam ring in 1982. The results presented here are based on the runs in the 1982-83 cycle. The center-of-mass energy was 29 GeV.

The topics covered in this paper are:

Results from the PEP-4 TPC on baryon production can be found in the contribution of Koichi Maruyama to this conference, and results from PEP-4/PEP-9 on two-photon interactions can be found in the contribution of Hans Sens.

2. PEP-4 TPC DETECTOR

The PEP-4 TPC detector is shown in Fig. 1, and the properties and operating conditions of its various subsystems are summarized in Table 1. The subsystems of the PEP-4 TPC detector include:

* TPC[1], which provides three-dimensional tracking and dE/dx particle identification.

* Drift chambers[2] at the inner and outer radii of the TPC, used primarily for triggering.

* Electromagnetic Calorimeters[3] with projective readout, both on the magnet pole tips and in six hexagonal modules around the magnet coil.

* Muon system[4], providing muon identification for particles that penetrate a one-meter iron filter.

Most of the results in this paper depend on the identification of particles by the TPC. This is done by a simultaneous measurement of momentum and dE/dx ionization energy loss for each particle. After a track passes through the TPC its ionization electrons drift axially to the endcaps, where they are detected in multiwire proportional chambers (sectors). As many as 183 dE/dx samples per track are obtained from the pulse heights. The ionization energy loss has a broad spectrum with a long high energy (Landau) tail. Many samples, therefore, are needed to define an effective dE/dx. In practice we define the dE/dx for each track to be the mean of the smallest 65% of the individual samples.

Figure 2 shows the distribution of dE/dx vs momentum for tracks in multihadron events, and the theoretical curves of expected dE/dx for various particle types. In the low-momentum region, the pion, kaon and proton bands are well separated; above 1 GeV/c the dE/dx resolution, 3.7%, is comparable to the separations in dE/dx for the above particle species. Figure 3 shows the ratio of measured dE/dx to that expected for pions for particles in the momentum range 3.5 to 6.0 GeV/c, after electron subtraction. The solid lines represent the contributions of pions, kaons and protons. The significance of the proton signal is more than five standard deviations.

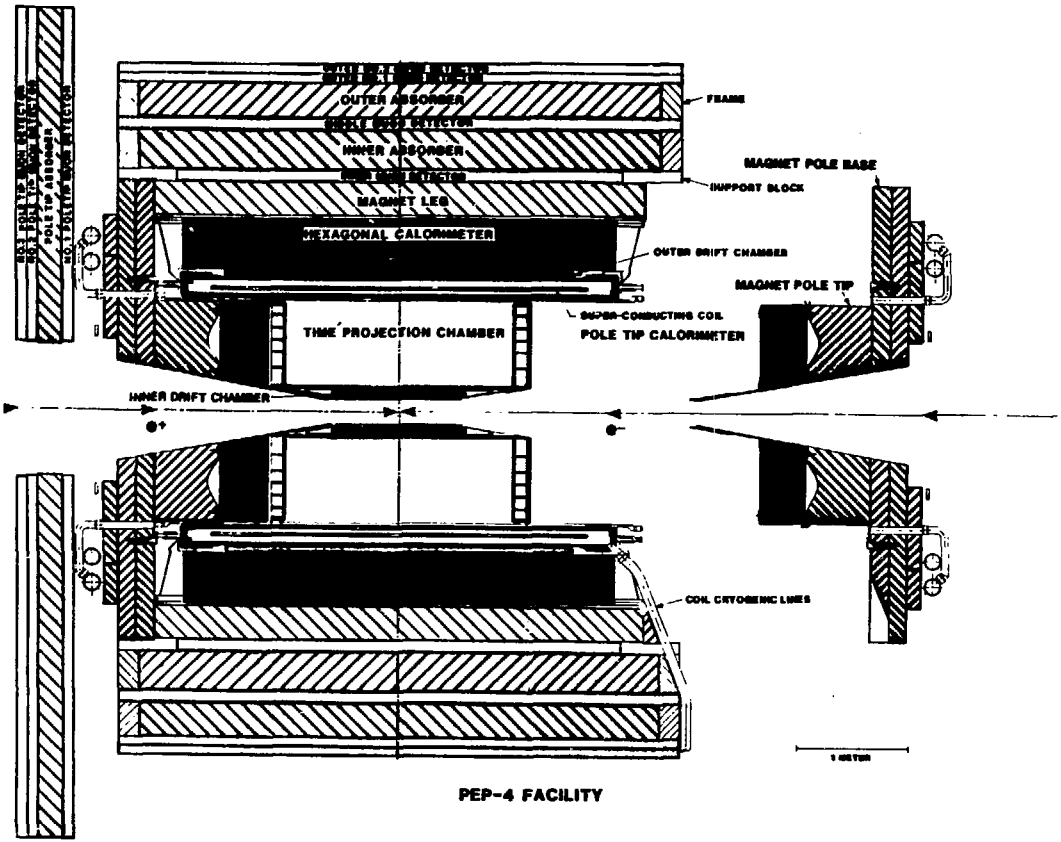

Fig. 1 The PEP-4 TPC Detector

Table 1. Summary of the PEP-4 TPC Detector Subsystems.

LOCATION	PEP e^+e^- ring, Interaction Region (IR) 2 SLAC, Stanford, CA, USA
MAGNET	1982–83: 4 kG Al coil solenoid ($1.32X_0$ coil package) 1984: 14.5 kG superconducting coil ($0.86X_0$ package) Diameter = 2.15 m, length = 3.0 m
TRACKING	Time Projection Chamber (TPC) 2.0 m long (in z) at 20 to 100 cm radius (r) Argon-methane (80%–20%) at 8.5 atm. Max. drift 1.0 m in 20 μsec, 75 kV/m drift electric field 183 proportional wire hits on tracks with $\|\cos\theta\| < 0.71$, each wire gives r,z and amplitude for six 60° sectors at each end and provides dE/dx meas. by multiple ionization sampling 15 3-dim. space points from induced cathode signals on several of 13,824 channels to give r, ϕ, and z (from the drift time), for $\|\cos\theta\| < 0.71$ ≥2 3-d points and ≥15 wire hits over 97% of 4π sterad Track pair resolution of 1–2 cm dE/dx ±3.5% for Bhabhas ±4.0% for tracks in jet events with ≥120 samples σ_p/p^2 = ±3.6% for p≥ 2 GeV/c position resolution in bending plane is 190 microns and in axial (z) direction 340 microns; presently low magnet field and drift distortions increase σ_p/p^2 Inner drift chamber at 13 to 19 cm radius 8.5 atm Ar-CH_4 (80%–20%), 150 microns in bend plane 1.2 m long covering 95% of 4π, with 4 axial layers Outer drift chamber at 1.19 to 1.24 m radius 1 atm Ar-CH_4 (80%–20%), 200 microns in bend plane 3 m long covering 77% of 4π, with 3 axial layers
POLE-TIP CALORIMETER	Gas, proportional mode, sampling Pb-laminate calorimeter 2 modules, $13.5X_0$ deep, at z = 1.1 m, covering 18% of 4π Argon-methane (80%–20%) at 8.5 atm; total of 51 samples Three 60° stereo views, each with 13 and 4 samples in depth *Projective strip geometry with 8 mrad angular segment* σ_E/E = ±11%/$\sqrt{E}$, below 10 GeV ±6.0% for Bhabhas at 14.5 GeV
HEXAGONAL CALORIMETER	Gas, limited Geiger mode, sampling Pb-laminate calorimeter 6 modules, $10X_0$ deep, 4.2 m long at 1.2 m radius Argon-ethyl bromide (96%–4%) at 1 atm. Solid angle coverage of 75% (90% including PTC) 3 correlated 60° stereo views using wire and cathode signals in 40 samples (27 and 13 samples in depth) Projective strip geometry with 9 mrad angular segment σ_E/E = ±14%/$\sqrt{E}$, below 1 GeV ±12% for Bhabhas at 14.5 GeV
MUON DETECTOR	Magnet flux return + 2 layers iron, total 810 g/cm Triangular, double layer, extruded Al proportional tubes Argon-methane (80%–20%) at 1 atm. 3 layers with axial wires and 4th layer at 90 deg. Endcap with 3 layers provides 98% of 4π sterad coverage Resolution = 1 cm, expect 3 mm when operated as drift tube
TRIGGER	≥2 charged over 85% of 4π sterad; neutral energy of ≥4 GeV, or energy in two or more calorimeter modules of ≥1.5 GeV; ≥1 charged and neutral energy of ≥750 MeV or energy in two or more calorimeter modules of ≥1.5 GeV

REFERENCES

1. TPC: H. Aihara et al., IEEE Trans. NS 30 (1983).
2. IDC: W. Gorn et al., IEEE Trans. NS 26 (1979) 67.
3. HEX: H. Aihara et al., IEEE Trans. NS 30 (1983).
4. MUON: J. Bakken et al., IEEE Trans. NS 30 (1983).
5. TRIG: M. Ronan et al., IEEE Trans. NS 29 (1982) 427.

3/83

XBL 845-1714

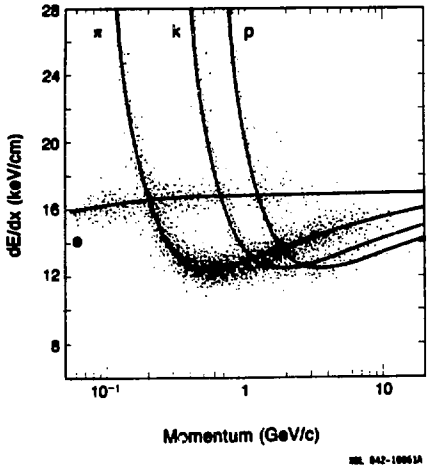

Fig. 2 Scatter plot of dE/dx vs momentum for tracks in a sample of multihadronic events, with the theoretical curves of expected dE/dx for various particle types.

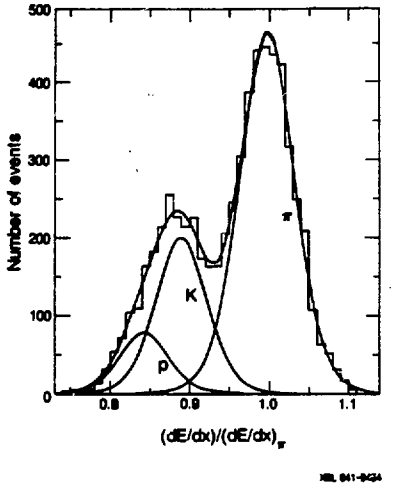

Fig. 3 The ratio of measured dE/dx to that expected for pions for particles in the momentum range 3.5 to 6.0 GeV/c, after electron subtraction. The solid lines represent the contributions of pions, kaons and protons.

3. EVENT SELECTION

The results presented in this paper are based on (except where noted) an integrated luminosity of 77 inverse picobarns, which corresponds to a sample of 29,094 multihadron events.

For the selection of multihadron events, charged tracks with momenta greater than 150 MeV/c and polar angle greater than 30 degrees are accepted as "good" if the extrapolated orbit passes the nominal interaction point within 10 cm in the beam direction and within 6 cm in the plane perpendicular to the beams. An event candidate must have at least 5 good charged tracks, not including electrons which are identified either by dE/dx or by geometrical reconstruction of the pairs from photon conversions. In order to eliminate two-photon and

beam-gas events, the total energy E(ch) of the charged particles (including electrons) must exceed one half the beam energy, and the sum of the momentum components along the beam direction must be less than 40% of E(ch)/c. Three-prong tau decays are removed by requiring that at least one jet in the event has either an invariant mass above 2 GeV or more than 3 non-electron tracks. With these cuts, backgrounds are estimated to be less than 1.5%. The event acceptance is 77% before radiative corrections.

We compare much of the data in this paper with the LUND model for quark and gluon fragmentation[5], and, as will be seen, the agreement is quite good. A similarly good agreement is obtained for independent-fragmentation schemes of the Feynman-Field type. The LUND model has simply been used as a representative of a wide class of models in which fragmentation distributions are essentially governed by longitudinal phase space for the directly produced objects, followed by resonance decays. We use LUND Version 5.2 ("Symmetrical LUND"), with the default values of the parameters. In particular:

* Production ratio of vector to pseudoscalar mesons (V/PS) = 1
* Production ratio of s to u quarks (s/u) = 0.3
* Production ratio of diquarks to quarks (qq/q) = 0.09

4. INCLUSIVE CHARGED AND NEUTRAL PARTICLE PRODUCTION

4.1 SEARCH FOR FRACTIONALLY CHARGED PARTICLES

Electron-positron annihilations at high energies can provide very sensitive tests of quark confinement. Thus it is of great value to search for Q=1/3 and 2/3 particles. Recently a model has been proposed[6] in which color triplets are confined, yet some states with higher-order representations of SU(3) color are unconfined. It is possible in this model to have a free Q=4/3 diquark.

Using dE/dx information, the TPC detector is well suited to look for stable

particles with charges Q=1/3, 2/3 or 4/3, as dE/dx ionization energy loss is proportional to the square of the charge. In Fig. 4, a scatter plot is shown of dE/dx vs apparent momentum (P/Q) for tracks in part of our multihadron sample, with lines showing the expected ionization curves for Q=1/3 (solid line), Q=2/3 (dashed line) and Q=4/3 (dot-dashed line) particles of mass 5 GeV. As the mass increases (decreases), all the curves move to the right (left). The apparent momentum (P/Q) arises because the analysis assumes a unit charge for fitted tracks. The searches for fractionally charged particles were performed in regions not populated by stable Q=1 particles (i.e. top and bottom right corners of Fig. 4). No candidate tracks were found in the lower search region. In the upper search region about 100 tracks were found, but these "tracks" were shown to result from pairs of nearby overlapping tracks which were reconstructed by the analysis software as single tracks, and thus appeared to have an anomalously large dE/dx. The fine spatial segmentation of the TPC allowed us to develop a series of cuts to eliminate this background,[7] based on the widths of the ionization clusters. These cuts resulted in no candidate tracks in the upper search region.

Figures 5, 6 and 7 show our limits[7,8] on inclusive production of stable Q=4/3, 2/3 and 1/3 particles in hadronic events, along with results of similar searches by other experiments.[9-12] Our Q=4/3 results are based on 22 inverse picobarns of data, and our other results on the full 77 inverse picobarns. The limits depend on the assumptions made for the production momentum spectrum and mass of the particles. The TPC results represent a substantial improvement on the previously established limits.

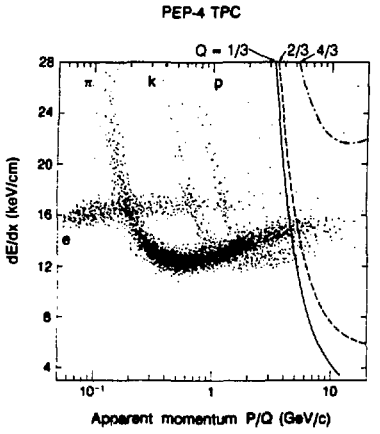

Fig. 4 Scatter plot of dE/dx vs apparent momentum (P/Q) for tracks in a sample of multi-hadronic events. The lines are the expected ionization curves for Q=1/3 (solid line), Q=2/3 (dashed line) and Q=4/3 (dot-dashed line) particles of mass 5 GeV.

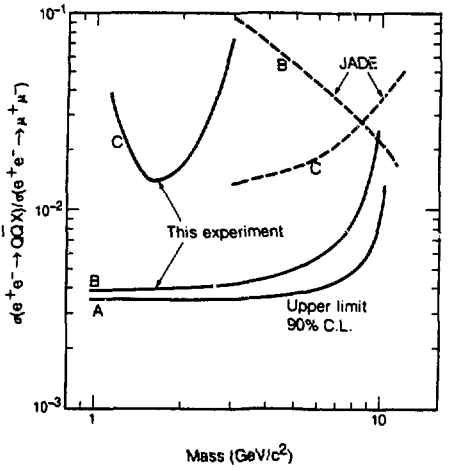

Fig. 5 Upper limit curves for $R_Q=\sigma(e^+e^-\to Q\bar{Q}X)/\sigma_{\mu\mu}$ for Q=4/3 particles. The assumed momentum distributions are A) $dN/dP \sim P^2/E$, B) dN/dP=constant, C) $dN/dP \sim (P^2/E)e^{-3.5E}$.

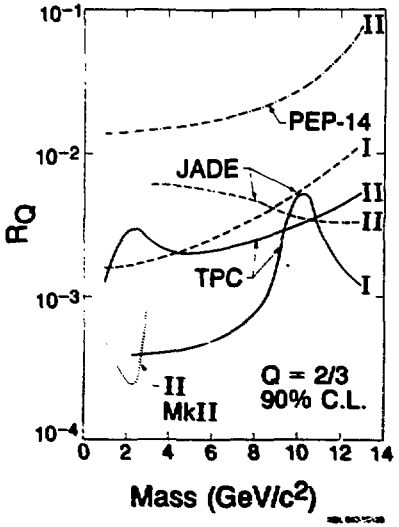

Fig. 6 Upper limit curves for $R_Q=\sigma(e^+e^-\to Q\bar{Q}X)/\sigma_{\mu\mu}$ for Q=2/3 particles. The assumed momentum distributions are I) $dN/dP \sim P^2/E$ II) $dN/dP \sim (P^2/E)e^{-3.5E}$.

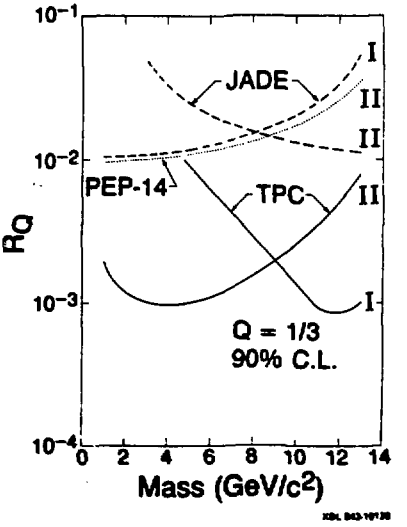

Fig. 7 Upper limit curves for $R_Q=\sigma(e^+e^-\to Q\bar{Q}X)/\sigma_{\mu\mu}$ for Q=1/3 particles. The assumed momentum distributions are I) $dN/dP \sim P^2/E$ II) $dN/dP \sim (P^2/E)e^{-3.5E}$.

4.2 CHARGED PARTICLE FRACTIONS AND CROSS-SECTIONS

Our understanding of the fragmentation of quarks and gluons into hadrons is enhanced by a knowledge of the production cross sections of charged pions, kaons and protons in e+e- annihilation at high energy. These particles were identified by dE/dx over the entire momentum range and over almost the entire solid angle using the TPC. This results in smaller systematic and statistical errors than previous measurements that used dE/dx at low momentum only,[13] or a combination of different methods such as time-of-flight or Cherenkov counters with limited acceptance.[14]

For the measurement of inclusive cross sections in the low momentum region, the raw numbers of pions, kaons and protons are obtained by counting tracks in the bands corresponding to the particle types (see Fig. 2). In the momentum regions close to and above minimum ionization, a maximum likelihood fit to the electron-subtracted dE/dx distribution is used. For a given momentum interval, we fit to a sum of three distributions (pions, kaons, and protons) whose relative peak positions and shapes are fixed (see Fig. 3). As input to this fit, we use the velocity dependence of the average dE/dx as determined from independent measurements of cosmic ray muons, conversion pairs and Bhabha electrons. From the same data the shape of the distribution of truncated means at a given velocity is parameterized.

The number of hadrons observed in each momentum bin is corrected for: geometrical acceptance, selection efficiency, decay, nuclear interactions, energy loss and initial state radiation.[15] Typical efficiencies are about 45%.

Figure 8 shows the fraction[16] of pions, kaons and protons among charged hadrons as a function of their momenta. The agreement with the LUND model (curves) is quite good. A production ratio of s to u quarks of 0.3, and a production ratio of diquarks to quarks of 0.09 were used in the model. Our measurements confirm the rise of the kaon and proton fractions with increasing momentum.

The normalized inclusive production cross sections[16] for pions, kaons and

protons are shown in Fig. 9. Again, the agreement with the LUND model is quite good. Within errors, the proton fractions and inclusive cross sections agree with earlier measurements from TASSO.[14] The kaon fractions and cross sections below 1 GeV/c are significantly lower than the TASSO data; at higher momenta the two experiments agree (see insert in Fig. 9). The inclusive pion cross sections agree within errors although the TPC data tends to be somewhat higher.

Mean hadron multiplicities have been determined using a fit to the production cross section by a sum of exponentials to extrapolate to momentum regions where no measurements are available. On the average an event contains 10.7±0.6 charged pions, 1.35±0.13 charged kaons, and 0.60±0.08 protons and anti-protons. The quoted uncertainties include systematic errors.

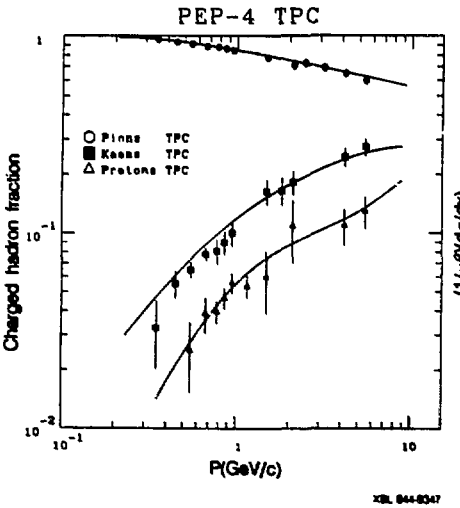

Fig. 8 Particle fractions vs momentum for pions, kaons and protons. For the lowest two momentum points the proton fraction was assumed to be 1%. The curves are the LUND model predictions.

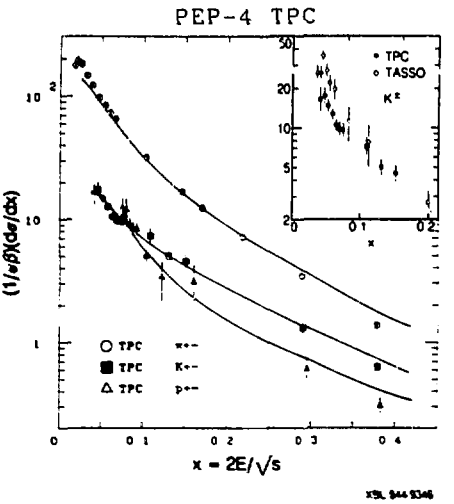

Fig. 9 Differential cross section vs x = E(hadrons)/14.5 GeV, for pions, kaons and protons. The curves are the LUND model predictions.

4.3. NEUTRAL PION PRODUCTION

In addition to charged hadron production we have measured neutral pion production using both photons from the hexagonal electromagnetic calorimeter (HEX) and pair conversion photons in the TPC.

The HEX[3] consists of six modules outside the magnet coil. For the data reported here (49 inverse picobarns) five of the six HEX modules were operational. Each module is 10 radiation lengths deep and contains 40 layers of a lead-fiberglass-aluminum laminate alternating with Geiger mode gas sampling gaps. Electromagnetic showers are reconstructed by matching the signals measured in a three view 60-degree stereo-projection system with 0.5-degree wide hodoscopic channels of sense wires and cathode strips.

A second method of photon reconstruction is provided by e+e- conversion pairs in the TPC. Approximately 20% of the primary photons convert in the material ahead of the TPC, mainly in the inner pressure wall. The kinematics for each pair-candidate are subjected to cuts requiring a minimum distance of approach, a minimum opening angle and a direction consistent with an origin at event vertex.

The photon inclusive cross sections determined by the two methods are in excellent agreement with one another. The fraction of the total center-of-mass energy carried by photons whose energy is between 0.1 and 6.5 GeV is measured to be 0.25±0.03. Below 0.1 GeV and above 6.5 GeV we estimate by smooth extrapolation that the additional contribution is about 0.01. The total fraction is then 0.26±0.03 (preliminary). The photon multiplicity in the energy range 0.1-6.5 GeV is 10.0±1.5.

Figure 10 shows the invariant mass distribution for all photon pair combinations in the HEX data for which each photon energy is greater than 0.4 GeV. This energy cut is imposed to reduce the background at low energy. The maximum likelihood fit to a background function plus Gaussian peak gives a pi-zero mass resolution of 28±1 MeV, consistent with what is expected with our photon energy and position resolutions. The acceptance for pi-zeros is

calculated by Monte Carlo simulation. It increases linearly from 0% at 0.8 GeV to 12% at 3.5 GeV, and decreases steeply at higher pi-zero energies because of the finite two photon resolution.

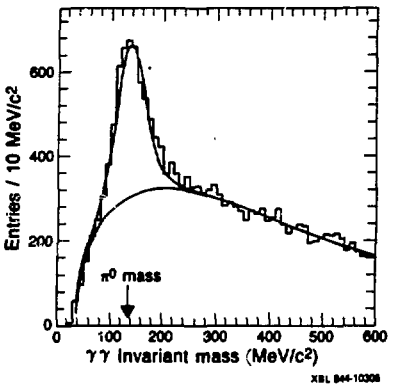

Fig. 10 Photon-photon invariant mass spectrum. The fitted curve is a Gaussian on a background shape estimated by Monte Carlo.

The preliminary pi-zero inclusive cross section is presented in Fig. 11a. The errors include statistical and systematic errors except for an overall 8% normalization uncertainty. The fraction of total center-of-mass energy carried by pi-zeros in our measurement range is 0.14±0.02. Monte Carlo programs[5] predict that the contribution below 1.0 GeV and above 6.4 GeV is 0.08±0.01. The total energy fraction is then 0.22±0.03 (preliminary). Each of the above energy fractions has systematic and statistical errors included. The pi-zero multiplicity in the energy range 1.0-6.4 GeV is 2.0±0.3. Figure 11a includes pi-zero cross section measurements from other experiments at comparable energies. Our cross sections agree with the measurements by TASSO[17] and CELLO[18] at 34 GeV.

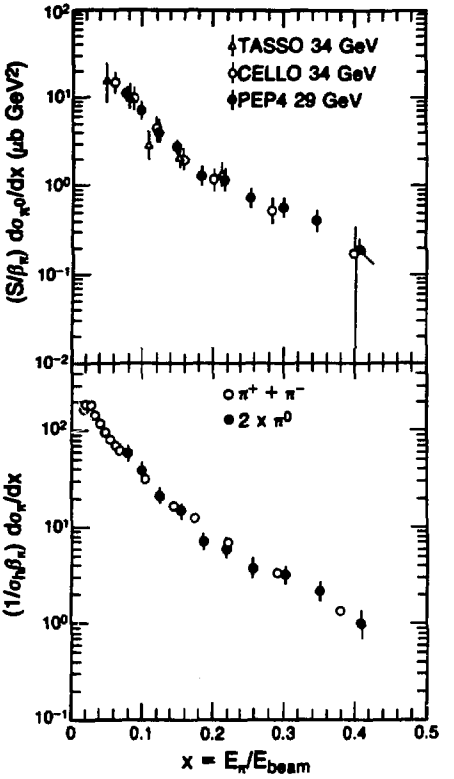

Fig. 11 Neutral pion inclusive cross section, compared with a) other measurements at similar energies, and b) the charged pion inclusive cross section measured using the same data sample.

In Fig. 11b, our pi-zero cross sections are compared with the average charged pion cross sections measured in the TPC with the same data sample.[16] In this case, systematic errors in the integrated luminosity and in the event selection efficiency cancel out. The measurements are consistent with equal yields of neutral and charged pions. In the range x=0.08-0.41, we find the ratio of the pi-zero to charged pion cross section to be 0.92±0.14. In a similar measurement at 34 GeV, TASSO[17] finds a neutral to charged pion ratio of 1.2±0.4 for pions in the range x=0.03-0.09.

5. PRODUCTION OF K* AND PHI MESONS

The investigation of resonance production in electron-positron annihilation at high energies provides important information on the mechanism of parton fragmentation. The interpretation of final state hadron data in terms of parton fragmentation is hindered by the fact that the shapes of the spectra may be dominated by decay products of heavier particles. The behaviors of vector mesons and other resonances are, on the other hand, more directly related to the quantum number and energy flow of the original partons and their hadronization. This analysis is based on 69 inverse picobarns of data.

In this study of neutral K* and phi meson production, the TPC was used to identify kaons and pions by dE/dx, and to reconstruct the decays: $K^* \rightarrow K^+ \pi^-$ (plus charge conjugate) and phi $\rightarrow K^+K^-$. The dE/dx identification in this case was done for each particle, as opposed to the statistical separation that was done in Section 4.2. For momenta where kaons cannot be identified unambiguously, the probability for a particle to be called a kaon was calculated from the difference of its measured dE/dx and the expected dE/dx for a kaon of that momentum. The probability was weighted with the measured charged kaon fraction (see Section 4.2), and a minimum value of this weighted probability was required for a particle to be called a kaon. The same procedure was used to identify pions.

Figure 12a shows the K+K- invariant mass distribution. A clear peak is observed in the phi mass region just above the K+K- threshold. No such structure is seen in the like-sign combinations of kaons, as shown in Fig. 12b. Fitting the distribution in Fig. 12a with a Gaussian line shape plus a smooth background gives 62.2±10.5 phis in the peak, M(K+K-)=1.019±0.002 GeV, and RMS width = 6.2±0.4 MeV which is consistent with the estimated detector resolution.

The scaled inclusive phi cross section[19] is shown in Fig. 13, along with the charged kaon cross section (see Section 4.2) and the K* cross section (to be discussed below). Also shown are the LUND model[5] predictions, using a production ratio of s to u quarks of 0.3. It is seen that the LUND model

prediction is consistent with the phi data. We obtain 0.077±0.012±0.016 phis/event for $0.075 < x < 0.55$, where $x = E(KK)/14.5$ GeV. Extrapolating to the full x range we obtain 0.084±0.013±0.018 for the total number of phis/event.

The transverse momentum distribution of phis relative to the event jet axis provides additional information on parton fragmentation, giving a measure of the transverse energy scale of hadronization. The phi production cross section as a function of the square of the transverse momentum relative to the event thrust axis is shown in Fig. 14 (filled circles). Included in Fig. 14 for comparison is the measured transverse momentum distribution of charged pions in the TPC, scaled by a factor of 1/140. The average value of the square of the transverse momentum for phi is 1.0±0.4 $(GeV/c)^2$. The Lund model predicts 0.85 $(GeV/c)^2$, and gives a reasonable fit to the measured spectra of both phi and pion. The average squared transverse momentum is larger for the phi than for the pion, suggesting that the phi spectrum is, as predicted, less dominated by the decay products of heavier particles.

Figure 15 shows the invariant mass distribution for unlike-sign kaon-pion combinations, where both the kaon and pion have been identified by the TPC using dE/dx. A clear peak is observed in the K* mass region, and no such structure is seen in the like-sign kaon-pion combinations. Fitting the distribution in Fig. 15 with a p-wave Breit-Wigner function plus a smooth background gives 2250±120 K*s in the peak, $M(K^+\pi^-)$=0.901±0.001 GeV, and full width = 0.082±0.001 GeV, which is consistent with the detector resolution. The background subtracted signal is also shown in Fig. 15.

The preliminary scaled inclusive neutral K* cross section is shown in Fig. 13, along with the charged kaon and phi cross sections. It is again seen that the LUND model prediction, with a vector to pseudoscalar production ratio of 1, is in good agreement with the data. Production ratios (V/PS) of 3 are clearly excluded. For $0.1 < x < 0.8$, where $x = E(K\pi)/14.5$ GeV, we measure 0.39±0.04±0.05 neutral K*s per event.

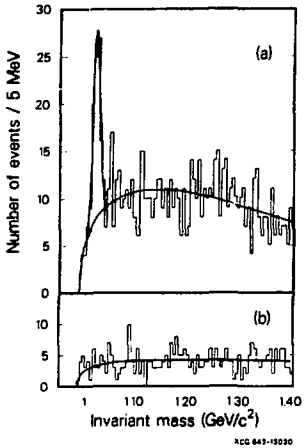

Fig. 12 a) K+K- invariant mass distribution. The fitted curve includes a Gaussian line shape plus a smooth background. b) Sum of the K+K+ and K-K- invariant mass spectra. The smooth curve shows a Monte Carlo prediction of the spectrum.

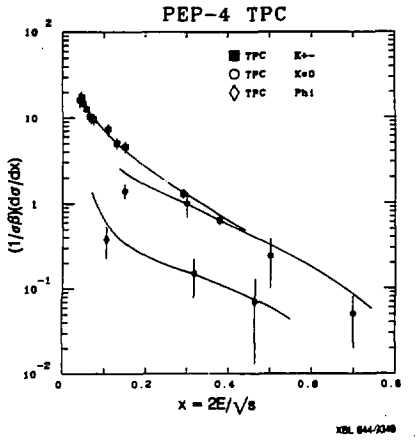

Fig. 13 Scaled inclusive cross section for charged kaons, neutral K* mesons and phi mesons. The curves are the LUND model predictions.

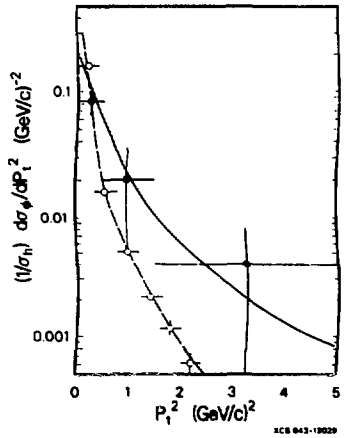

Fig. 14 Distribution of the square of the phi transverse momentum with respect to the thrust axis (filled circles). The open circles give the distribution observed for charged pions, scaled by a factor of 1/140 for comparison. The curves are the LUND model predictions.

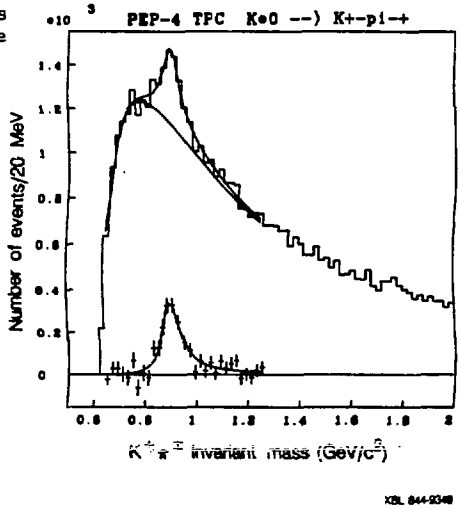

Fig. 15 $K^{\pm}\pi^{\mp}$ invariant mass distribution. The fitted curve includes a Breit-Wigner function plus a smooth background.

6. HEAVY QUARK FRAGMENTATION

6.1 DIRECT ELECTRON PRODUCTION

Prompt leptons serve as a clean signal of heavy (c and b) quarks. The lepton production rates and momentum spectra reflect the semileptonic branching fractions and energy spectra of the parent hadrons containing the heavy quarks. The distribution of transverse momentum with respect to the thrust axis depends on the parent quark mass, making it possible to separate b quark events from c quark events. Using the charge of the prompt lepton to distinguish quark jets from antiquark jets, we can measure the forward-backward asymmetry in e+e- annihilations into quarks. Our results using direct electrons are described in this section, and with direct muons in the next section.

Electrons are identified by both the TPC (using dE/dx) and the HEX electromagnetic calorimeter. For a track to be identified as an electron in the HEX, its energy must agree with the TPC-momentum, and the lateral shape of the shower must be consistent with the shape expected for electrons. Combining the TPC and HEX measurements, the hadron misidentification probability is 0.003-0.3%, depending on momentum. The major background is due to electrons from photon conversions in the material (0.2 r.l.) in front of the TPC, and from Dalitz decays. About 70% of these backgrounds are removed by geometrical reconstruction of e+e- pairs. The electron acceptance and identification efficiency, determined using both a Monte Carlo simulation and photon conversion electrons, is about 70% for the TPC and 60% for the HEX.

Figure 16 shows momentum distributions of the 819 prompt electron candidates with $P > 0.5$ GeV/c, for $Pt < 1$ GeV/c and $Pt > 1$ GeV/c. Also shown are the distributions for electrons from photon conversions and Dalitz decays, and from misidentified hadrons, estimated by Monte Carlo. It is seen that hadron background is very low. The background-subtracted data are corrected for the geometrical acceptance, the electron identification efficiency and the hadronic event selection efficiency including the initial state radiative corrections. Figure 17 shows our inclusive cross sections[20] and those from previous

measurements.[21] Our measurements, which cover a very wide momentum range, agree with the previous ones.

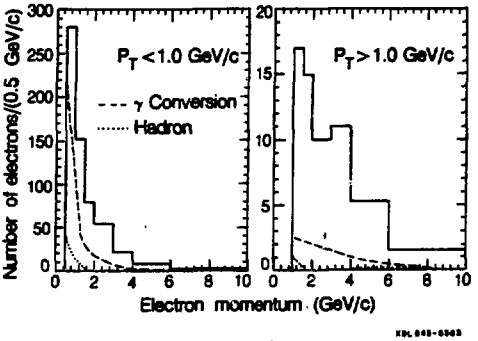

Fig. 16 Momentum spectrum of electrons (solid line) with estimated remaining backgrounds due to electrons from photon conversions and Dalitz decays (dashed line), and due to hadrons (dotted line).

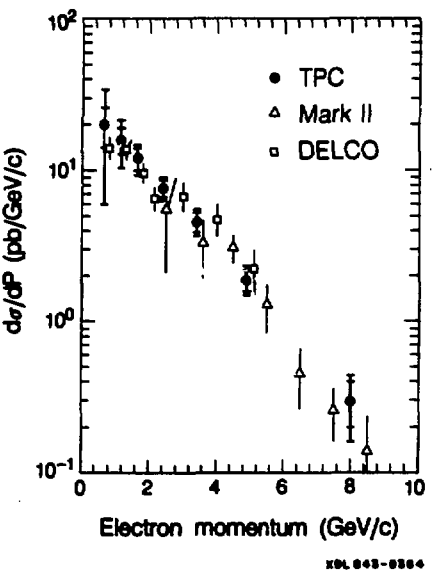

Fig. 17 Differential cross section vs momentum for direct electrons, compared with other measurements.

To obtain semielectronic branching fractions of hadrons containing c and b quarks and the shape of the b quark fragmentation function, we perform a two-dimensional maximum-likelihood fit to the distribution of electrons in P and Pt bins. The data are fitted with the contribution from primary ($b \to e$) and secondary ($b \to c \to e$) b quark decays, primary ($c \to e$) c quark decays and the background. Two different forms for the fragmentation function are used--that of Peterson et al.[22] and Andersson et al.[5] We fix the parameters of the c quark fragmentation function by fitting the D* scaling cross sections measured at PEP and PETRA[23] (*epsilon = 0.24 in the Peterson formula*). The function of Peterson et al. yields the c and b quark semielectronic branching fractions, BR(c) = (9.1±0.9±1.3)% and BR(b) = (11.0±1.8±1.0)%, respectively. The b quark fragmentation function peaks at high z=E(hadron)/E(beam) with $\langle z \rangle = 0.74 \pm 0.05 \pm 0.03$. The function of Andersson et al. gives almost identical results. The background subtracted momentum distributions are shown in Fig. 18, along with the fitted contributions from the b and c quark decays.

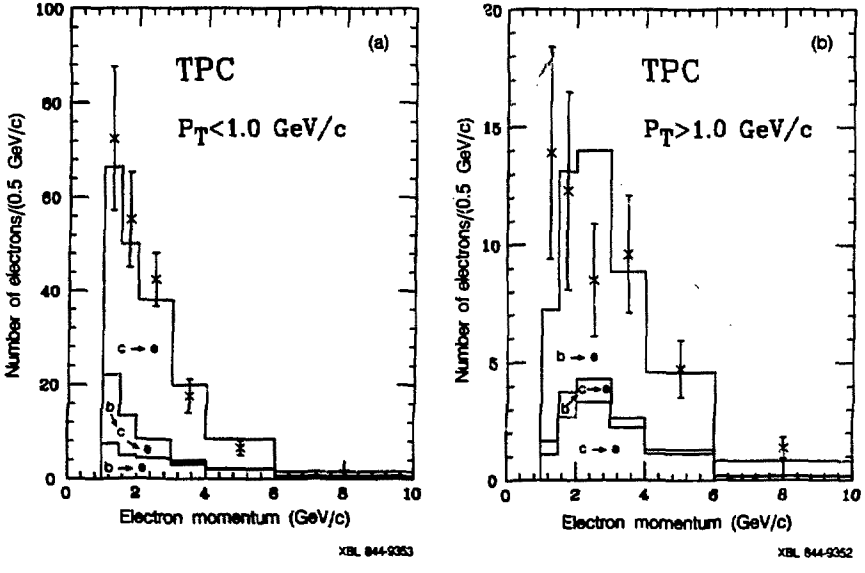

Fig. 18 Momentum spectrum of electrons (with background subtracted), along with the fitted contributions from b and c quark decays.

In order to measure the forward-backward asymmetry, we define c-enriched ($P>1.5$ GeV/c, $Pt<1.0$ GeV/c) and b-enriched ($P>1.5$ GeV/c, $Pt>1.0$ GeV/c) samples. There are 270 events in the c-enriched sample and 80 events in the b-enriched sample. Figure 19 shows the background-subtracted and acceptance-corrected distribution of the angle between the incident electron and the thrust axis for the c-enriched and b-enriched samples. The forward direction of the thrust axis is defined to be in the hemisphere containing the prompt electron or the opposite of the hemisphere containing the prompt positron. The angular distribution is parameterized as $(1+\cos^2\theta+\lambda\cos\theta)$, where lambda is a measure of the forward-backward asymmetry. In the standard electroweak theory[24] lambda is proportional to the axial vector coupling of a quark to the neutral weak current, a(q), divided by the quark charge. To determine a(c) and a(b), we perform a maximum-likelihood fit to the angular distributions of both samples simultaneously, taking into account the relative contributions from quark decays and background. The results are $a(c)=2.3\pm1.4\pm1.0$ and $a(b)=-2.0\pm1.9\pm0.5$, consistent with the standard model expectations of +1 and -1, respectively.

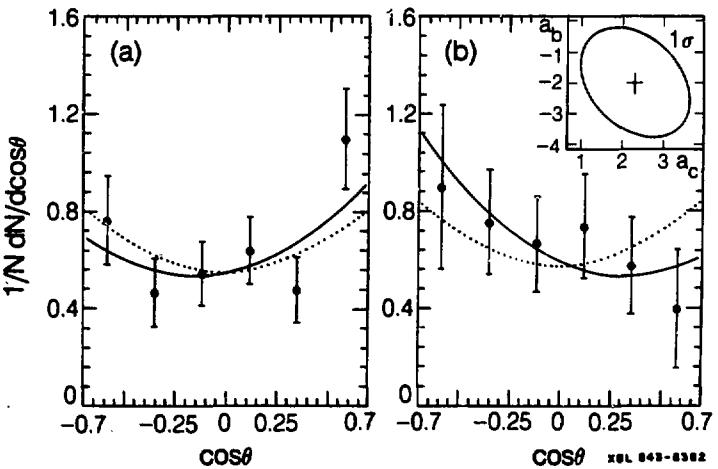

Fig. 19 Background-subtracted and acceptance-corrected angular distributions of the thrust axis for a) c-enriched sample, b) b-enriched sample. The solid curve indicates the fit with $1+\cos^2\theta+\lambda\cos\theta$. The dotted curve is proportional to $1+\cos^2\theta$. The insert in (b) shows the equal-likelihood contour of 1 s.d. in the a(c)-a(b) plane.

6.2 DIRECT MUON PRODUCTION

The measurement of prompt muons in e+e- annihilation, as with direct electrons, yields information on the semi-leptonic branching ratios of the heavy c and b quarks, their fragmentation functions, and their forward-backward asymmetries.

In the PEP-4 detector, particles are identified as muons by using four layers of triangular shaped proportional chambers to sample a track's path four times through one meter of iron. For this analysis, muon candidates were tracks with momenta greater than 2 GeV/c, polar angle greater than 55 degrees, and unambiguous hits in all four muon chamber layers. Each layer is 99.6% efficient, so the total inefficiency of the last requirement is less than 2%. The major background is due to hadron punch-through and decay-in-flight, which is calculated by Monte Carlo. The final sample has 982 muon candidates, with an estimated background of 38%.

As was done with the electron data, a two-dimensional maximum-likelihood fit was done to the distribution of muons in P and Pt bins, including contributions from c and b quark decays. The Peterson et al. fragmentation function was used. The c and b quark semimuonic branching fractions from the fit are $BR(c)=(7.2\pm1.4\pm0.5)\%$ and $BR(b)=(13.2\pm1.8\pm1.0)\%$. The b quark fragmentation function is found to peak at high $z=E(\text{hadron})/E(\text{beam})$ with $\langle z\rangle=0.83\pm0.05\pm0.03$, in agreement with the direct electron results, and the c quark fragmentation function is found to be softer with $\langle z\rangle=0.55\pm0.07\pm0.03$. The preliminary background subtracted momentum distributions are shown in Fig. 20, along with the fitted contributions from the b and c quark decays.

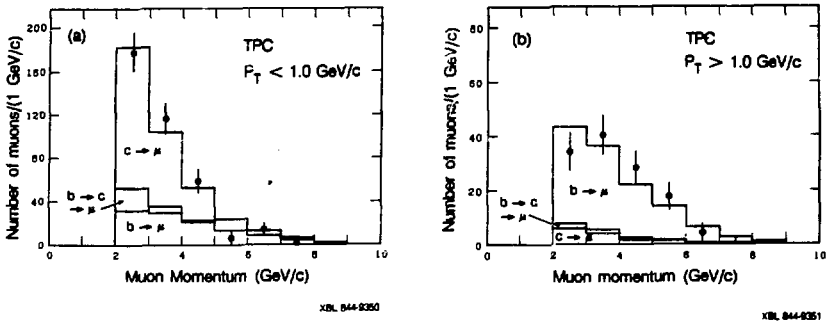

Fig. 20 Momentum spectrum of muons (with background subtracted), along with the fitted contributions from b and c quark decays.

6.3 D* PRODUCTION

Some very recent results are available from PEP-4 on D* production, using the well established technique of using the narrow D*-D mass difference to tag D*s. The D* is studied via its decay $D^{*+} \to D^0\pi^+$, with the D^0 decaying into $K^-\pi^+$, $K^-\pi^+\pi^-\pi^+$ and $K^-\pi^+\pi^0$. The charged kaons and pions are identified by the TPC using dE/dx, as described in Section 5, and the neutral pions are identified using the HEX calorimeter, as described in Section 4.3.

For the $K\pi$ decay channel of the D, one requires that the invariant mass of the $K\pi$ combination be within 250 MeV of the D mass, and that the cosine of the decay angle of the K in the $K\pi$ rest frame be less than 0.8. Similar cuts are made for the other D decay channels. Since the sign of the K is known, $K\pi$ pairs are combined only with pions having the "right" sign (i.e. opposite to that of the K) to form D* candidates, and the mass difference, $\Delta = M(K\pi\pi)-M(K\pi)$, is then calculated. Similar combinations are made for the other D decay channels.

The preliminary distribution of the D*-D mass difference obtained by the above technique is shown in Fig. 21, for all three decay modes of the D. Fitting the distribution with a Gaussian function plus a smooth background gives about 120 D*s. The preliminary inclusive normalized cross section (i.e. fragmentation function) of the D*s is shown in Fig. 22. The fragmentation function peaks at around $z=E(D^*)/E(beam)=0.6$.

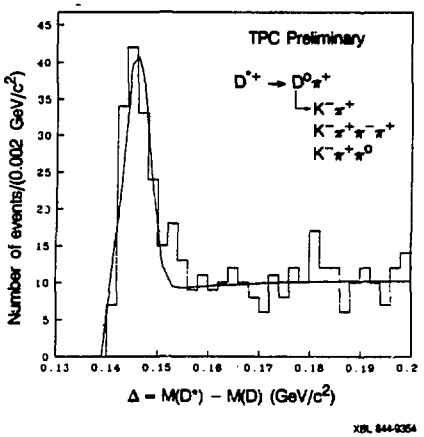

Fig. 21 Mass difference $\Delta = M(D^*) - M(D)$, for all three decay modes of the neutral D meson.

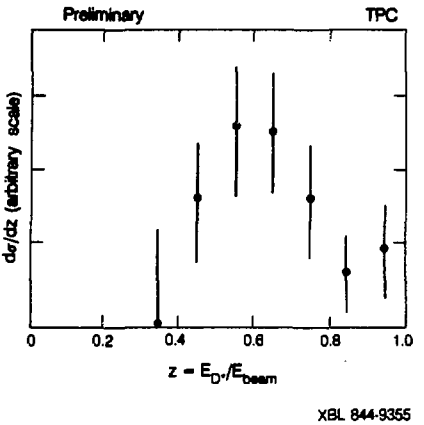

Fig. 22 Normalized inclusive charged D* cross section.

7. FLAVOR CORRELATIONS

Standard models of hadronization divide the process of e+e- annihilation into hadrons into two distinct regimes. First, the production of a parton (q-qbar) system is dominated by perturbative theory. Second, on a much longer timescale, the non-perturbative strong interactions transform these partons into observable hadrons (fragmentation). These two regimes can be examined by studying flavor correlations in jetlike events.

A particle's rapidity is defined as $y=0.5 \ln (E+Pl)/(E-Pl)$, where Pl is the momentum parallel to the jet axis of the event. For 2-jet events, the leading particles of one jet have $Pl > 0$ (and thus $y > 0$), and the leading particles of the other jet have $Pl < 0$ (and $y < 0$). Thus particles in opposite jets usually have large rapidity differences, and correlations between these particles are called long range correlations (LRC). LRC provide evidence for the existence of flavor carrying initial partons (quarks). Particles in the same jets usually have small rapidity differences, and correlations between these particles are called short range correlations (SRC). SRC show local conservation of quantum numbers (like charge and flavor) in the fragmentation process.

The motivation for studying flavor correlations is twofold. In the case of SRC, it is difficult to separate correlations due to the fragmentation process from those due to resonance decays. Since only a few resonances decay into two kaons (most notably the phi), correlations between kaons provide more information on the fragmentation process than pion correlations do. In the case of LRC, flavor correlations provide interesting information on the production and fragmentation of heavy quarks.

The kaons and pions used in these flavor correlation studies were identified by the TPC using dE/dx, in a manner similar to that described in Section 5. The K purity is greater than 75% for all rapidity values, and the pion purity is greater than 90%.

For the flavor correlation analysis, one first determines the jet axis (using sphericity) for each multihadron event, and then calculates the rapidities of all the particles with respect to this axis. A "test particle" of type "a" (a=K for kaon, Pi for pion) in a given rapidity range is chosen. For all other identified particles of type "b" and rapidity y in the event, the flavor tagged charge density, D(ab), is calculated for each y value:

D(ab) = (Number of "b" particles of opposite charge to test particle "a")
- (Number of "b" particles of same charge as test particle "a")

D(ab) is then normalized to the total number of test particles.

In Figs. 23a,b,c, we present preliminary distributions of D(PiPi), D(KK) and D(PiK) versus y. For these three plots the rapidity of the "test particle" was in the range 1.5-4. The distributions have been corrected for acceptance using values obtained by running annihilation events generated by the Lund Monte Carlo, with radiative corrections,[15] through a detector simulation. These corrections are functions not only of rapidity but of the angle of the measured sphericity axis with respect to the beamline as well, since for a given angle the loss of tracks down the beamline results in a localized dip in acceptance. The distributions are also corrected for particle misidentification. The error bars include systematic uncertainties associated with these corrections.

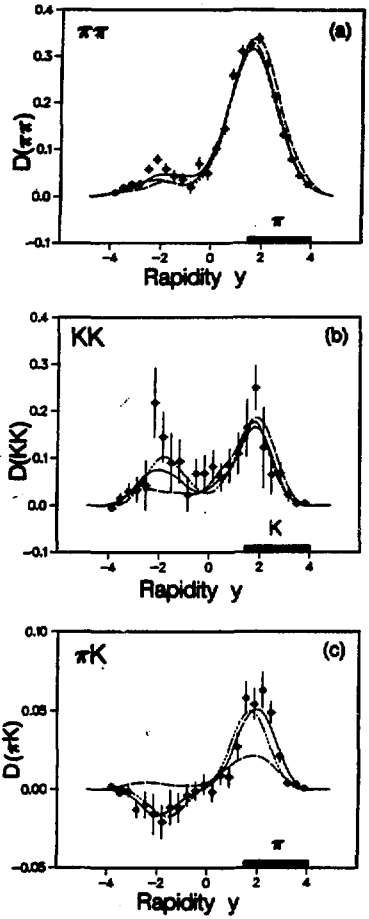

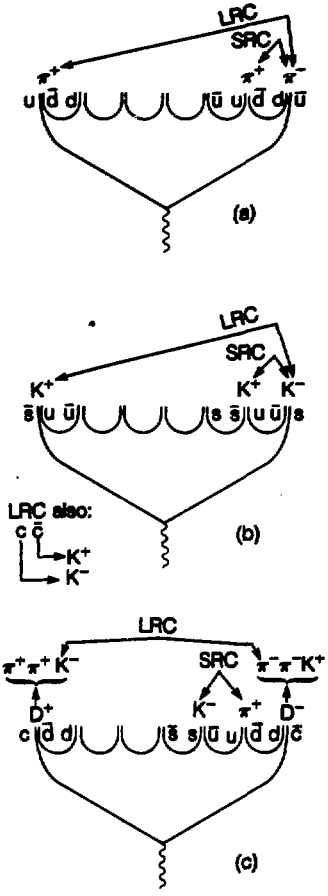

XBL 844-9345

Fig. 23 Flavor tagged charge density, D(ab), vs rapidity y.
a) D(PiPi) b) D(KK)
c) D(PiK). The rapidity of the test particle "a" was 1.5-4. The solid line shows the prediction of the LUND model (with c and b quarks). The dashed line shows the prediction of the LUND model without c and b quarks. The dot-dashed line shows the prediction of the Webber model.

Fig. 24 Some mechanisms responsible for long range (LRC) and short range (SRC) correlations.
a) PiPi b) KK c) PiK.

The Pi-Pi correlations in Fig. 23a are quite similar to the charge compensation results presented previously by other experiments.[25,26] There is a large SRC due to resonance decays and local charge conservation during fragmentation, as is schematically shown in Fig. 24a. A smaller LRC is seen, which provides evidence for the presence of charged primary partons (see Fig. 24a). Integrating the distribution shows that 95±2% of the pion charge is compensated by another pion.

The K-K correlations (Fig. 23b) are qualitatively similar to those for Pi-Pi, but there are clear differences between them. The relative strength of the SRC and LRC are comparable in the K-K case, while for the Pi-Pi case the SRC is stronger than the LRC by about a factor of 4. Integrating the K-K distribution gives a value of 62±9%. This value, considerably smaller than the value for the Pi-Pi case, is consistent with the fact that approximately half of the strangeness is carried by neutral kaons. Mechanisms which can give K-K SRC and LRC are shown schematically in Fig. 24b.

The impact of heavy quark decays is dramatically seen in the Pi-K correlations (Fig. 23c). Unlike the other two distributions, D(Pi-K) shows a significant same charge (rather than opposite charge) LRC. This LRC is a result of decays like $c \to \pi^+ K^-$ and $\bar{c} \to \pi^- K^+$ on opposite ends of the jet (see Fig. 24c). Heavy quark decays play an important role in determining the shape of the long range Pi-Pi and K-K correlations as well. The solid line in Fig. 23 shows the prediction of the "symmetric" Lund model. The dashed line shows the prediction of the model without heavy (charm and bottom) quarks. The model gives better agreement with the data in the standard configuration where heavy quarks are included. The dot-dashed line shows the prediction of the Webber model,[27] with heavy quarks, which also is in agreement with the data.

8. SUMMARY

New results from the PEP-4 TPC, many of which use particle identification by dE/dx ionization energy loss in the TPC, have been presented.

A search has been done for stable particles of fractional charge Q=1/3, 2/3 and 4/3. No candidates have been found, and the TPC results represent a substantial improvement over previously established limits.

The production cross sections of charged pions, kaons and protons have been measured up to a momentum of 7 GeV/c. Mean hadron multiplicities have been determined for these particle types.

Neutral pion and photon production have been studied using the TPC and HEX calorimeter. We have measured the fraction of the total energy carried by neutral pions and photons, and have verified that the neutral pion differential cross section agrees well with our corresponding measurement for charged pions, as expected from isospin symmetry.

The investigation of resonances provides additional information on the mechanism of parton fragmentation. Using TPC identified kaons and pions we have very clean phi and neutral K* signals. We have measured the phi and K* inclusive cross sections,. and the number of phis and K*s per event. We find that the transverse momentum distribution of the phi is harder than that of pions, suggesting that the phis are closer to the primary hadronic production than the pions, which are mostly decay products of resonances.

Prompt leptons serve as a clean signal of heavy (c and b) quarks. Using the TPC and HEX calorimeter we have obtained a sample of direct electrons where hadrons have been rejected by a factor of 10,000 or more. Using this sample we have measured the inclusive prompt electron cross section over a wide momentum range. We have also measured the semielectronic branching ratios of c and b quarks, the b quark fragmentation function, and the axial vector couplings of c and b quarks to the weak neutral current.

Using the PEP-4 muon detector, we have determined the semimuonic branching ratios of c and b quarks, and the c and b quark fragmentation functions. All

muon results agree well with the electron results.

We have obtained a sample of about 120 D*s by using the well established technique of using the narrow D*-D mass difference to tag D*s. A preliminary D* fragmentation function has been measured with this sample.

We have studied charge weighted correlations in rapidity space for TPC identified kaons and pions. Of particular interest are K-K correlations, which exhibit both long range and short range strangeness compensation. In addition, we observe significant K-Pion correlations as a result of heavy (c and b) quark decays.

We acknowledge the efforts of the PEP staff, and the engineers, programmers and technicians of the collaborating Institutions who made this work possible. This work was supported by the U.S. Department of Energy under contract numbers DE-AC03-76SF00098, DE-AM03-76SF00034, and DE-AC02-76ER03330, the National Science Foundation and the Joint Japan-U.S. Collaboration in High Energy Physics.

REFERENCES

1. PEP-4 TPC Collaboration, H. Aihara et al., IEEE Trans.Nucl.Sci. NS30, 63, 76, 162 (1983); N.J.Hadley, Ph.D. thesis, LBL-16116 (1983); R.Z.Fuzesy, N.J.Hadley and P.R.Robrish, LBL-16808 (1983).

2. PEP-4 TPC Collaboration, H.Aihara et al., IEEE Trans.Nucl.Sci. NS-30 153 (1983); W. Gorn et al., IEEE Trans.Nucl.Sci. NS-26, 68 (1979).

3. PEP-4 TPC Collaboration, H.Aihara et al., Nucl.Instr. and Meth. 217, 259 (1983); PEP-4 TPC Collaboration, H.Aihara et al., IEEE Trans.Nucl.Sci. NS-30, 117 (1983); A.Barbaro-Galtieri et al., Nucl.Instr. and Meth. 213, 223 (1983).

4. PEP-4 TPC Collaboration, H.Aihara et al., IEEE Trans.Nucl.Sci. NS-30, 67 (1983); J.A.Bakken, Ph.D. thesis, The Johns Hopkins University (1983); D.H. Badtke et al., Nucl.Instr. and Meth. 188, 497 (1981).

5. B.Andersson et al., Phys.Rep. 97, 31 (1983); B.Andersson, G.Gustavson and B.Soederberg, Z.Phys. C20, 317 (1983).

6. R.Slansky, T.Goldman, and G.Shaw, Phys.Rev.Lett. 47, 887 (1981). See also A.De Rujula, R.Giles, and R.Jaffe, Phys.Rev.D 17, 285 (1978).

7. PEP-4 TPC Collaboration, H.Aihara et al., Phys.Rev.Lett. 52, 168 (1984).

8. PEP-4 TPC Collaboration, H.Aihara et al., LBL-17551 (1984), submitted to Physical Review Letters.

9. JADE Collaboration, W.Bartel el al., Z.Phys. C 6, 295 (1980).

10. J.Burger, Proc.Int. Symposium on Lepton and Photon Interactions at High Energies, edited by W.Pfeil (Univ. of Bonn, 1981), p.115.

11. Mark II Collaboration, J.M.Weiss et al., Phys.Lett. 101B, 439 (1981).

12. PEP-14 Collaboration, M.C.Ross et al., Phys.Lett. 118B, 199 (1982).

13. JADE Collaboration, W.Bartel et al., Phys.Lett. 104B, 325 (1981).

14. TASSO Collaboration, M.Althoff et al., Z.Phys. C17, 5 (1983).

15. F.A.Berends and R.Kleiss, Nucl.Phys. B178, 141 (1981).

16. PEP-4 TPC Collaboration, H.Aihara et al., Phys.Rev.Lett. 52, 577 (1984).

17. TASSO Collaboration, R.Brandelik et al., Phys.Lett. 108B, 71 (1982).

18. CELLO Collaboration, H.J.Behrend et al., Z.Phys. C20,207 (1983).

19. PEP-4 TPC Collaboration, H.Aihara et al., LBL-17616 (1984), submitted to Physical Review Letters.

20. PEP-4 TPC Collaboration, H.Aihara et al., LBL-17545 (1984), submitted to Physical Review Letters.

21. Mark II Collaboration, M.E.Nelson et al., Phys.Rev.Lett. 50, 1542 (1983); DELCO Collaboration, D.E.Koop et al., SLAC-PUB-3266 (1983), to be published in Physical Review Letters.

22. C.Peterson et al., Phys.Rev. D27, 105 (1983).

23. Mark II Collaboration, J.M.Yelton et al., Phys.Rev.Lett. 49, 430 (1982); TASSO Collaboration, M. Althoff et al., Phys.Lett. 126B, 493 (1983); HRS Collaboration, S.Ahlen et al., Phys.Rev.Lett. 51, 1147 (1983).

24. S.Weinberg, Phys.Rev.Lett. 19, 1264 (1967); A. Salam, Proc. 8th Nobel Symp., ed. N.Svartholm (Almqvist and Wiksell, Stockholm, 1968) p.367; J.Ellis and M.K.Gaillard, CERN-76-18 (1976)21.

25. TASSO Collaboration, R. Brandelik et al., Phys.Lett. 100B, 357 (1981).

26. ACCDHW Collaboration, D. Drijard et al., Nucl.Phys. 166B, 233 (1980).

27. B. Webber, CERN-TH-3713 (1983).

This report was done with support from the Department of Energy. Any conclusions or opinions expressed in this report represent solely those of the author(s) and not necessarily those of The Regents of the University of California, the Lawrence Berkeley Laboratory or the Department of Energy.

Reference to a company or product name does not imply approval or recommendation of the product by the University of California or the U.S. Department of Energy to the exclusion of others that may be suitable.